Numerical Simulation of Incompressible Fluid Flow using Locally Solenoidal Elements

O. KARAKASHIAN
Dept. Of Mathematics, University of Tennessee
Knoxville, TN 37996-1300, U.S.A.
ohannes@math.utk.edu

TH. KATSAOUNIS
Dept. Of Applied Mathematics, University Of Crete and IACM
FORTH, Heraklion, Crete, Greece
thodoros@tem.uoc.gr

Abstract—In this paper, we present a numerical study of the performance of a discontinuous Galerkin formulation for the Navier-Stokes equations. This method is characterized by the fact that the velocity field is approximated using piecewise polynomial functions that are totally discontinuous across interelement boundaries and which are pointwise divergence-free on each element (locally solenoidal). In particular, numerical results are presented for two well-known benchmark problems. © 2006 Elsevier Ltd. All rights reserved.

Keywords—Incompressible flow, Solenoidal elements, Discontinuous Galerkin method.

1. INTRODUCTION

We consider the stationary Navier-Stokes equations for viscous incompressible flow as given in the primitive variable formulation,

$$-\nu\Delta\mathbf{u} + (\mathbf{u}\cdot\nabla)\mathbf{u} + \nabla p = \mathbf{f} \qquad \text{in } \Omega, \tag{1}$$

$$\operatorname{div}\mathbf{u} = 0 \qquad \text{in } \Omega, \tag{2}$$

$$\mathbf{u} = \mathbf{g} \qquad \text{on } \partial\Omega. \tag{3}$$

Here, $\mathbf{u} = (u_1,\ldots,u_N) : \Omega \to R^N$ represents the velocity field, and $p : \Omega \to R$, the pressure; the function $\mathbf{f} = (f_1,\ldots,f_N) : \Omega \to R^N$ denotes the prescribed external body forces, $\mathbf{g} = (g_1,\ldots,g_n) : \partial\Omega \to R^N$, the admitted flux across the boundary $\partial\Omega$ and $\nu > 0$ is a constant measuring viscosity. Note that $\mathbf{g}$ must satisfy the compatibility condition $\int_{\partial\Omega} \mathbf{g}\cdot\mathbf{n}\,d\sigma = 0$.

One of the attributes of the numerical method presented herein is the use of totally discontinuous piecewise polynomial vector functions to approximate the velocity field $\mathbf{u}$. These functions

satisfy the incompressibility condition (2) pointwise on each element of a partition of Ω. A special weak formulation is designed to account for the interelement jumps that ensue. The weak form includes penalty jump terms designed to enforce continuity in a weak sense, [1,2]. This is common practice in discontinuous Galerkin methods, [3–5]. Recently, Oden and Baumann introduced a method which dispenses with such terms and achieves stability by reversing the sign of one of the terms in the bilinear form, cf., [6] and the references therein. For the pressure, standard continuous piecewise polynomial functions are used. For the method that we shall describe below, a range of theoretical issues including the stability and convergence of the approximations at the optimal rates were presented in [2]. These results extended those obtained in [1] for the Stokes problem. Also, in [7], the application of implicit Runge-Kutta methods to the corresponding time dependent problem were analyzed.

Continuing our earlier work, [8], we present a much more expanded set of numerical experiments designed to gauge the performance of our method and to offer a study of its characteristics. For the sake of completeness, we include in Section 2 needed expository material borrowed from [2] and [8]. This includes a description of the energy spaces, the discontinuous Galerkin formulations and enumeration of some relevant analytical results. Section 3 contains the new material in this paper. It describes some implementational aspects of the method and includes data confirming the convergence rates established in [1] and [2]. The two benchmark problems of the driven cavity and backward facing step provide an important test for our approach and allow a comparison with other available methods.

2. PRELIMINARIES

2.1. The Energy Spaces

We shall next construct appropriate settings for the velocity, the pressure and their approximations as well as the Galerkin formulation. To begin, we consider partitions $\mathcal{T}_k = \{\Omega_1, \ldots, \Omega_{d_k}\}$ of Ω parameterized by $k > 0$. For simplicity, we shall use the generic name of element to denote Ω_i, which will be typically a triangle in 2-D or a tetrahedron in 3-D. We note that our formulation allows for more general shapes. In particular, the outlying elements may have a curved edge or face if Ω is not polygonal.

The formal setting for the velocity will be provided by the (mesh-dependent) "energy" space $\mathbf{E}_k = \mathbf{H}^2(\Omega_1) \times \cdots \times \mathbf{H}^2(\Omega_{d_k})$, where $\mathbf{H}^2$ is the Sobolev space of index 2 (cf., [9]). We may view $\mathbf{E}_k$ as a subspace of $\mathbf{L}^2(\Omega)$. In addition to the L^2 norm, we equip $\mathbf{E}_k$ with the mesh-dependent H^1-like norm,

$$
\|\mathbf{v}\|_{1,k} = \left\{ \sum_{i=1}^{d_k} \left(\|\nabla \mathbf{v}^{(i)}\|_{\Omega_i}^2 + \sum_{j \in \mathcal{N}_i} \tau_{ij} \left[k_i \left| \frac{\partial \mathbf{v}^{(i)}}{\partial n} \right|_{\partial \Omega_{i,j}}^2 + k_i^{-1} \left| \mathbf{v}^{(i)} - \mathbf{v}^{(j)} \right|_{\partial \Omega_{i,j}}^2 \right] \right. \right.
$$
$$
\left. \left. + k_i \left| \frac{\partial \mathbf{v}^{(i)}}{\partial n} \right|_{\partial \Omega_i^e}^2 + k_i^{-1} \left| \mathbf{v}^{(i)} \right|_{\partial \Omega_i^e}^2 \right) \right\}^{1/2},
$$

(4)

where

- k_i is the diameter of $\partial \Omega_i$,
- $\partial \Omega_{i,j} = \partial \Omega_i \cap \partial \Omega_j$, if $\partial \Omega_i$ and $\partial \Omega_j$ are adjacent,
- $\partial \Omega_i^e = \partial \Omega_i \cap \partial \Omega$,
- $\mathbf{v}^{(i)}$ is the restriction of $\mathbf{v}$ to $\partial \Omega_i$,
- $\mathbf{v}^{(i)} - \mathbf{v}^{(j)}$ denotes the jump in $\mathbf{v}$ across $\partial \Omega_{i,j}$,
- $\frac{\partial \mathbf{v}^{(i)}}{\partial n}$ is the normal derivative of $\mathbf{v}^{(i)}$ with respect to the unit outward normal to $\partial \Omega_i$,
- $\mathcal{N}_i = \{j : \Omega_j \text{ is adjacent to } \Omega_i\}$,
- $\tau_{ij} = 1$ if $i > j$ and $\tau_{ij} = 0$ if $i \leq j$.

Further, we denote

$$(\mathbf{u},\mathbf{v})_D = \int_D \mathbf{u}\cdot\mathbf{v}\,dx = \sum_{i=1}^N \int_D u_i v_i\,dx, \qquad \|\mathbf{v}\|_D = (\mathbf{v},\mathbf{v})_D^{1/2},$$

$$(\mathbf{u},\mathbf{v}) = (\mathbf{u},\mathbf{v})_\Omega,$$

$$\langle\mathbf{u},\mathbf{v}\rangle_\Gamma = \int_\Gamma \mathbf{u}\cdot\mathbf{v}\,ds = \sum_{i=1}^N \int_\Gamma u_i v_i\,ds, \qquad \text{edge or surface integrals,}$$

$$|\mathbf{v}|_\Gamma = \langle\mathbf{v},\mathbf{v}\rangle_\Gamma^{1/2}.$$

To approximate the pressure, we use a partition $\mathcal{T}_h = \{\Omega_1^h,\ldots,\Omega_{d_h}^h\}$ of Ω possibly different from $\mathcal{T}_k$. In order to satisfy the Babuska-Brezzi stability condition establishing the compatibility of the velocity and pressure finite-element spaces, we shall assume that $\mathcal{T}_k$ is possibly finer than $\mathcal{T}_h$ in the sense that every element Ω_ℓ^h is a union of members of $\mathcal{T}_k$.

Since the pressure is determined up to an additive constant only, it is convenient to work with quotient spaces X/R obtained by identifying all functions in the space X that differ by constants. Such a space is $L^2(\Omega)/R$. (Note that equivalently one could work with the space $L_0^2(\Omega) = \{q \in L^2(\Omega) : \int_\Omega q\,dx = 0\}$). $L^2(\Omega)/R$ is a Banach space when equipped with the quotient norm $\|q\|_{L^2(\Omega)/R} = \inf_{c\in R}\|q-c\|_{L^2(\Omega)}$. We shall also use the following mesh-dependent and L^2-like norm on the quotient space $H^1(\Omega)/R$,

$$\|q\|_{0,h} = \left\{\|q\|_{L^2(\Omega)/R}^2 + \sum_{\ell=1}^{d_h} h_\ell^2\|\nabla q^{(\ell)}\|_{\Omega_\ell^h}^2\right\}^{1/2},$$

where h_ℓ is the diameter of Ω_ℓ^h.

2.2. The Finite-Element Spaces

The set of vector functions,

$$\left\{\begin{pmatrix}1\\0\end{pmatrix}, \begin{pmatrix}0\\1\end{pmatrix}, \begin{pmatrix}y\\0\end{pmatrix}, \begin{pmatrix}0\\x\end{pmatrix}, \begin{pmatrix}x\\-y\end{pmatrix}\right\},$$

forms a basis for the space of linear solenoidal functions in R^2. Augmenting it by

$$\left\{\begin{pmatrix}y^2\\0\end{pmatrix}, \begin{pmatrix}0\\x^2\end{pmatrix}, \begin{pmatrix}x^2\\-2xy\end{pmatrix}, \begin{pmatrix}-2xy\\y^2\end{pmatrix}\right\},$$

gives a basis for quadratics. In R^3, for $r_1 = 2$, a basis is given by the set,

$$\left\{\begin{pmatrix}1\\0\\0\end{pmatrix}, \begin{pmatrix}0\\1\\0\end{pmatrix}, \begin{pmatrix}0\\0\\1\end{pmatrix}, \begin{pmatrix}0\\x\\0\end{pmatrix}, \begin{pmatrix}0\\0\\x\end{pmatrix}, \begin{pmatrix}y\\0\\0\end{pmatrix}, \begin{pmatrix}0\\0\\y\end{pmatrix}, \begin{pmatrix}z\\0\\0\end{pmatrix}, \begin{pmatrix}0\\z\\0\end{pmatrix}, \begin{pmatrix}x\\-y\\0\end{pmatrix}, \begin{pmatrix}x\\0\\-z\end{pmatrix}\right\}.$$

It is typical in constructing finite-element spaces to use affine transformations to map "master" basis functions to each element Ω_i. It turns out however that the incompressibility property is not preserved by general affine transformations. Therefore, the local basis functions are constructed by translations and scaling of the above functions. We denote the finite-element space thus obtained by $\mathbf{V}_k^{r_1}$ where $r_1 - 1$ is the degree of the polynomials used. The fact that the spaces-$\mathbf{V}_k^{r_1}$ possess optimal approximations properties is established in [1].

To approximate the pressure, we use spaces $P_h^{r_2}$ of continuous piecewise polynomial functions of degree $r_2 - 1, r_2 \geq 2$ defined on the partition $\mathcal{T}_h$. These spaces are quite standard cf., [10].

2.3. The Discontinuous Galerkin Formulations

We begin by defining the bilinear form $a_k^\gamma(\cdot, \cdot) : \mathbf{E}_k \times \mathbf{E}_k \to R$

$$
\begin{aligned}
a_k^\gamma(\mathbf{u}, \mathbf{v}) = \sum_{i=1}^{d_k} \Bigg\{ (\nabla \mathbf{u}^{(i)}, \nabla \mathbf{v}^{(i)})_{\Omega_i} + \sum_{j \in \mathcal{N}_i} \tau_{ij} \Bigg[-\left\langle \frac{\partial \mathbf{u}^{(i)}}{\partial n}, \mathbf{v}^{(i)} - \mathbf{v}^{(j)} \right\rangle_{\partial \Omega_{i,j}} \\
-\left\langle \frac{\partial \mathbf{v}^{(i)}}{\partial n}, \mathbf{u}^{(i)} - \mathbf{u}^{(j)} \right\rangle_{\partial \Omega_{i,j}} + \gamma k_i^{-1} \left\langle \mathbf{u}^{(i)} - \mathbf{u}^{(j)}, \mathbf{v}^{(i)} - \mathbf{v}^{(j)} \right\rangle_{\partial \Omega_{i,j}} \Bigg] \\
-\left\langle \frac{\partial \mathbf{u}^{(i)}}{\partial n}, \mathbf{v}^{(i)} \right\rangle_{\partial \Omega_i^e} - \left\langle \frac{\partial \mathbf{v}^{(i)}}{\partial n}, \mathbf{u}^{(i)} \right\rangle_{\partial \Omega_i^e} + \gamma k_i^{-1} \left\langle \mathbf{u}^{(i)}, \mathbf{v}^{(i)} \right\rangle_{\partial \Omega_i^e} \Bigg\},
\end{aligned}
\tag{5}
$$

which constitutes a weak formulation for the Dirichlet integral $(\nabla \mathbf{u}, \nabla \mathbf{v})$. Indeed, if $\mathbf{u} \in \mathbf{H}^2(\Omega)$, then $\forall\, \mathbf{v} \in \mathbf{E}_k$

$$
a_k^\gamma(\mathbf{u}, \mathbf{v}) = -(\Delta \mathbf{u}, \mathbf{v}) - \sum_{i=1}^{d_k} \left\langle \mathbf{u}^{(i)}, \frac{\partial \mathbf{v}^{(i)}}{\partial n} - \gamma k_i^{-1} \mathbf{v}^{(i)} \right\rangle_{\partial \Omega_i^e}.
\tag{6}
$$

Some further comments on the nature of the form a_k^γ are in order as follows.

1. The first, second, and fifth terms on the right side of (5) are byproducts of integration by parts and range over the interior and boundary edges of $\mathcal{T}_k$, respectively. The array τ_{ij} is used to ensure that each interior edge is visited only once. This device is also convenient as a method for relating the ordering of the edges in a natural way to the ordering of the elements Ω_i.

2. The third and sixth terms have been added to ensure symmetry of the form a_k^γ. Note that the third term is zero for smooth $\mathbf{u}$, while the sixth is a known quantity since $\mathbf{u}|_{\partial \Omega}$ is given. We note that the theoretical results remain valid if these terms are removed.

3. The fourth and seventh are so-called "penalty" terms which, upon choosing γ sufficiently large, induce coercivity of the form a_k^γ. The choice of γ is independent of the partition $\mathcal{T}_k$.

The next few results highlight the analysis presented in [1] and [2]. In particular, the role of the penalty parameter γ is exhibited.

PROPOSITION 1.

(i)
$$
|a_k^\gamma(\mathbf{u}, \mathbf{v})| \leq (1 + \gamma) \|\mathbf{u}\|_{1,k} \|\mathbf{v}\|_{1,k}, \qquad \forall\, \mathbf{u}, \mathbf{v} \in \mathbf{E}_k.
$$

(ii) *There exist positive constants γ_0 and c_a such that for all $\gamma \geq \gamma_0$,*

$$
a_k^\gamma(\mathbf{v}, \mathbf{v}) \geq c_a \|\mathbf{v}\|_{1,k}^2, \qquad \forall\, \mathbf{v} \in \mathbf{V}_k^{r_1}.
$$

The value of γ_0 depends on r_1 but is independent of the meshsize k. Indeed, the bilinear form a_k^γ is singular if γ is small. It is interesting to note that recently a class of related of methods which discard the penalty terms have been proposed cf., [6]. In these methods, the bilinear form is made nonsingular by what essentially amounts to changing the sign of the third term on the right side of (5).

PROPOSITION 2. *There exists a constant $c > 0$, such that*

$$
(\mathbf{v}, \nabla q) \leq c \|\mathbf{v}\|_{1,k} \|q\|_{0,h}, \qquad \forall\, \mathbf{v} \in \mathbf{E}_k, \quad \forall\, q \in H^1(\Omega).
$$

THEOREM 1. *Let $r_1 \geq 1$ and $r_2 \geq 2$ be given. Suppose $\mathcal{T}_k$ is sufficiently fine with respect to $\mathcal{T}_h$. Then, there exists a positive constant c, independent of k and h, such that*

$$\sup_{0 \neq \mathbf{v} \in \mathbf{V}_k^{r_1}} \frac{(\mathbf{v}, \nabla q)}{\|\mathbf{v}\|_{1,k}} \geq c \|q\|_{0,h}, \qquad \forall q \in P_h^{r_2}. \tag{7}$$

This is the crucial Babuska-Brezzi (inf-sup) condition. Existence and convergence of the numerical approximations depend on it in an essential manner. It is a simple exercise in linear algebra to show that if (7) holds then we must necessarily have that $\dim \mathbf{V}_k^{r_1} \geq \dim P_h^{r_2} - 1$. In this sense, using discontinuous elements for the velocity in conjunction with continuous elements for the pressure constitutes a step in the right direction. Indeed, taking $\mathcal{T}_k$ fine with respect to $\mathcal{T}_h$ is a way of increasing the dimension of $\mathbf{V}_k^{r_1}$ with respect to the dimension of $P_h^{r_2}$. By the same token, (7) cannot hold for arbitrary choices of r_1 and r_2 without taking $\mathcal{T}_k$ finer than $\mathcal{T}_h$. However, our numerical experiments, all conducted with $r_1 = r_2$ or $r_1 = r_2 + 1$, suffered no apparent ill effects from taking $\mathcal{T}_k = \mathcal{T}_h$. We conjecture that (7) holds under these conditions.

At this point, we draw attention to similarities between our method and others in the literature. Indeed, in view of the fourth term in (5), our method can be termed as an "interior penalty" formulation. Such methods have been extensively studied in the context of elliptic and other types of problems [3–5,11,12]. In addition, the fact that the inf-sup property (7) holds for arbitrary choices of r_1 and r_2, provided of course, we choose $\mathcal{T}_k$ finer than $\mathcal{T}_h$, relates our method in spirit to so-called stabilized methods cf., [13,14].

We next construct a Galerkin approximation to the Stokes problem which is the system (1)–(3) minus the convective term $(\mathbf{u} \cdot \nabla)\mathbf{u}$. Multiplying (1) by $\mathbf{v} \in \mathbf{E}_k$ and integrating, we obtain after using (6),

$$\nu a_k^\gamma(\mathbf{u}, \mathbf{v}) + (\mathbf{v}, \nabla p) = (\mathbf{f}, \mathbf{v}) - \nu \sum_{i=1}^{d_k} \left\langle \frac{\partial \mathbf{v}^{(i)}}{\partial n} - \gamma k_i^{-1} \mathbf{v}^{(i)}, \mathbf{g} \right\rangle_{\partial \Omega_i^e}. \tag{8}$$

Now, multiplying (2) by $q \in H^1(\Omega)$ and integrating by parts and using the fact the solution of (1)–(3) is in $H^2(\Omega)$, we see that

$$(\mathbf{u}, \nabla q) = \langle \mathbf{g} \cdot \mathbf{n}, q \rangle_{\partial \Omega}. \tag{9}$$

Combining the last two equations, we derive the following weak formulation for the Stokes problem

$$\nu a_k^\gamma(\mathbf{u}, \mathbf{v}) + (\mathbf{v}, \nabla p) + (\mathbf{u}, \nabla q) = F_S([\mathbf{v}, q]), \qquad \forall [\mathbf{v}, q] \in \mathbf{E}_k \times H^1(\Omega), \tag{10}$$

$$F_S([\mathbf{v}, q]) = (\mathbf{f}, \mathbf{v}) - \nu \sum_{i=1}^{d_k} \left\langle \frac{\partial \mathbf{v}^{(i)}}{\partial n} - \gamma k_i^{-1} \mathbf{v}^{(i)}, \mathbf{g} \right\rangle_{\partial \Omega_i^e} + \langle \mathbf{g} \cdot \mathbf{n}, q \rangle_{\partial \Omega}. \tag{11}$$

Hence, we define the Galerkin approximation to the Stokes problem as the unique element $[\mathbf{u}_k, p_h] \in \mathbf{V}_k^{r_1} \times P_h^{r_2}/R$ satisfying

$$\nu a_k^\gamma(\mathbf{u}_k, \mathbf{v}) + (\mathbf{v}, \nabla p_h) + (\mathbf{u}_k, \nabla q) = F_S([\mathbf{v}, q]), \qquad \forall [\mathbf{v}, q] \in \mathbf{V}_k^{r_1} \times P_h^{r_2}/R. \tag{12}$$

To handle the convective term $(\mathbf{u} \cdot \nabla)\mathbf{u}$, we define the trilinear form $b_1(\cdot, \cdot, \cdot) : \mathbf{E}_k^3 \to R$ by

$$b_1(\mathbf{u}, \mathbf{v}, \mathbf{w}) = \sum_{i=1}^{d_k} \left\{ \int_{\Omega_i} u_\ell^{(i)} \frac{\partial v_m^{(i)}}{\partial x_\ell} w_m^{(i)} \, dx - \sum_{j \in \mathcal{N}_i} \tau_{ij} \int_{\partial \Omega_{i,j}} u_\ell^{(i)} (v_m^{(i)} - v_m^{(j)}) w_m^{(i)} n_\ell^{(i)} \, d\sigma \right\}, \tag{13}$$

where we have adopted Einstein's summation convention for repeated indices for components of vectors. Following a well known device of Témam, we introduce the skew-symmetric form,

$$b(\mathbf{u}, \mathbf{v}, \mathbf{w}) = \frac{1}{2} \left[b_1(\mathbf{u}, \mathbf{v}, \mathbf{w}) - b_1(\mathbf{u}, \mathbf{w}, \mathbf{v}) \right]$$

Note that we have $b(\mathbf{u}, \mathbf{v}, \mathbf{v}) = 0$, $\forall \mathbf{u}, \mathbf{v} \in \mathbf{E}_k$. Additionally, the following consistency result holds.

PROPOSITION 3. *Suppose* **u** *is in* $\mathbf{H}^2(\Omega)$ *and satisfies* div **u** = **0** *in* Ω. *Then,*

$$b(\mathbf{u}, \mathbf{u}, \mathbf{v}) = \int_{\Omega} ((\mathbf{u} \cdot \nabla)\mathbf{u})\mathbf{v}\, dx - \frac{1}{2} \int_{\partial\Omega} (\mathbf{u} \cdot \mathbf{n})(\mathbf{u} \cdot \mathbf{v})\, d\sigma, \qquad \forall\, \mathbf{v} \in \mathbf{E}_k.$$

The Galerkin approximation of the stationary Navier-Stokes problem (1)–(3) is defined as the unique solution $[\mathbf{u}_k, p_h] \in \mathbf{V}_k^{r_1} \times P_h^{r_2}/R$ of

$$\nu a_k^{\gamma}(\mathbf{u}_k, \mathbf{v}) + (\mathbf{u}_k, \nabla q) + (\mathbf{v}, \nabla p_h) + b(\mathbf{u}_k, \mathbf{u}_k, \mathbf{v}) \tag{14}$$

$$= F_{NS}[\mathbf{v}, q], \qquad \forall\, [\mathbf{v}, q] \in \mathbf{V}_k^{r_1} \times P_h^{r_2}/R, \tag{15}$$

$$F_{NS}[\mathbf{v}, q] = F_S([\mathbf{v}, q]) - \frac{1}{2} \langle \mathbf{g} \cdot \mathbf{n}, \mathbf{g} \cdot \mathbf{v} \rangle_{\partial\Omega}. \tag{16}$$

The convergence of the numerical approximations defined above is analyzed in [1] and [2]. Let [**u**, *p*] denote the solution of either the stationary Stokes or Navier-Stokes problems and assume it to be sufficiently smooth. For simplicity, suppose that $k = h$ and that $r_1 = r_2 = r$. Then, under certain conditions, (cf., [1,2] for details) the Galerkin approximations [$\mathbf{u}_k, p_h$] converge to [**u**, *p*] and satisfy the optimal rates

$$\|\mathbf{u} - \mathbf{u}_k\|_{L^2} + h\|\mathbf{u} - \mathbf{u}_k\|_{1,k} + h\|p - p_h\|_{0,h} \leq ch^r.$$

3. NUMERICAL RESULTS

In this section, we describe the numerical and implementational issues pertaining to the solution of the Stokes as well as the Navier-Stokes problem. In the first part, we shall concentrate on the implementation of the method, while in the second part, we consider the numerical validation of the various theoretical results, in particular the verification of the optimal convergence rates. Additionally, there are issues which are best illuminated by means of actual numerical experiments. For instance, it is important to determine whether taking the same mesh for the velocity and the pressure would cause the crucial inf-sup condition to break down. Even more significant is the experimental determination of a useful range of values for the parameter γ.

Finally, in the third part of this section, we apply our method to two well known benchmark problems, namely, the driven cavity and backward facing step problems.

3.1. Implementation

First, a triangulation of Ω is generated using the Modulef library [15]. The triangles are enumerated and other appropriate data structures are established. The various arrays and vectors are constructed using suitable basis functions. Those for the velocity are as described in Section 2.2. For the pressure, we use standard Lagrangian nodal basis functions expressed locally in terms of barycentric coordinates [10].

Let $\{\Phi_\ell\}_{\ell=1}^{J_u}$ be a basis for $\mathbf{V}_k^{r_1}$ and let $\{\psi_\ell\}_{\ell=1}^{J_p}$ be a basis for $P_h^{r_2}$. Writing $\mathbf{u}_k = \sum_{\ell=1}^{J_u} a_\ell \Phi_\ell$ and $p_h = \sum_{\ell=1}^{J_p} b_\ell \psi_\ell$ the Galerkin formulation (12) for the Stokes problem results in the linear system,

$$\begin{pmatrix} \nu S & B \\ B^T & 0 \end{pmatrix} \begin{pmatrix} \mathbf{a} \\ \mathbf{b} \end{pmatrix} = \begin{pmatrix} \bar{f} \\ \bar{g} \end{pmatrix}, \tag{17}$$

where

$$S_{ij} = a_k^{\gamma}(\Phi_i, \Phi_j), \qquad\qquad\qquad i, j = 1, \ldots, J_u,$$

$$B_{ij} = (\Phi_i, \nabla\psi_j), \qquad\qquad\qquad i = 1, \ldots, J_u, \quad j = 1, \ldots, J_p,$$

$$\bar{f}_j = (\mathbf{f}, \Phi_j) - \nu \sum_{i=1}^{d_k} \left\langle \frac{\partial \Phi_j^{(i)}}{\partial n} - \gamma k_i^{-1} \Phi_j^{(i)}, \mathbf{g} \right\rangle_{\partial\Omega_i^e}, \qquad j = 1, \ldots, J_u,$$

$$\bar{g}_j = \langle \mathbf{g} \cdot \mathbf{n}, \psi_j \rangle_{\partial\Omega}, \qquad\qquad\qquad j = 1, \ldots, J_p.$$

To solve the linear system (17), we adopted an algorithm devised by Bramley [16]. Indeed, it turned out to be the most efficient among several we tested, [7]. We describe briefly its derivation. For simplicity, we assume that $\bar{g} = 0$, $\nu = 1$. We solve (17) for $\mathbf{b}$ in the least squares sense, $\mathbf{b} = B^{\dagger}(\bar{f} - S\mathbf{a})$ where $B^{\dagger}$ is the Moore-Penrose pseudoinverse of B and substituting $\mathbf{b}$ with this in(17), we get

$$PS\mathbf{a} = P\bar{f}$$

where $P = I - BB^{\dagger}$ is the orthogonal projection onto $\ker(B^{T})$. On the other hand $B^{T}\mathbf{a} = 0$ if and only if $\mathbf{a} = P\mathbf{a}$, so

$$PSP\mathbf{a} = P\bar{f}.$$

The method now applies the standard conjugate gradient method to $PSP\mathbf{a} = P\bar{f}$. Assuming that B has full rank then $P = I - B(B^{\mathsf{T}}B)^{-1}B^{\mathsf{T}}$. The matrix $B^{\mathsf{T}}B$ is symmetric positive definite and its dimension is small compared to that of S. We notice also that for the time-dependent problem, B does not depend on time so $B^{\mathsf{T}}B$ can be factored once at the beginning.

In this method, if the projection P is computed exactly, then the residual of $B^{\mathsf{T}}\mathbf{a} = 0$ is zero and the method tries to bring the residual of $S\mathbf{a} + B\mathbf{b} = f$ to zero iteratively. Finally, a preconditioned conjugate gradient method, with preconditioner $PS^{-1}P$ can be used to solve $PSP\mathbf{a} = P\bar{f}$.

The Galerkin formulation (14) for the stationary Navier-Stokes problem is, on the other hand, nonlinear. We solve it using Newton's method, which takes the form,

$$
\begin{aligned}
\nu a_k^\gamma \left(\mathbf{u}_k^{(\ell+1)}, \mathbf{v} \right) + \left(\mathbf{u}_k^{(\ell+1)}, \nabla q \right) + \left(\mathbf{v}, \nabla p_h^{(\ell+1)} \right) \\
+ b \left(\mathbf{u}_k^{(\ell+1)}, \mathbf{u}_k^{(\ell)}, \mathbf{v} \right) + b \left(\mathbf{u}_k^{(\ell)}, \mathbf{u}_k^{(\ell+1)}, \mathbf{v} \right) \\
= b \left(\mathbf{u}_k^{(\ell)}, \mathbf{u}_k^{(\ell)}, \mathbf{v} \right) + F_{NS} \left([\mathbf{v}, q] \right), \quad \forall [\mathbf{v}, q] \in \mathbf{V}_k^{r_1} \times P_h^{r_2}, \qquad \ell = 0, \dots,
\end{aligned}
\tag{18}
$$

with $[\mathbf{u}_k^{(0)}, p_h^{(0)}]$ given. We found it efficient to take as $[\mathbf{u}_k^{(0)}, p_h^{(0)}]$ the solution of the corresponding Stokes problem. Then, we iterate until $\|\mathbf{u}_k^{(\ell+1)} - \mathbf{u}_k^{(\ell)}\| \leq \text{TOL}$. Indeed, in view of the asymptotic quadratic convergence of Newton's method, this will ensure that $\|\mathbf{u}_k - \mathbf{u}_k^\ell\| \leq \text{TOL}$, where TOL is a prescribed tolerance parameter.

3.2. The Stokes Problem

We consider first the linear Stokes problem. In all the experiments conducted in this part as well as for the Navier-Stokes problem, we took Ω to be the unit square. To perform a study of the errors and the convergence rates, we employed the following two functions.

Test Function #1 (F1)

$$
\begin{aligned}
\mathbf{u} &= \frac{1}{\pi^2} \left(\sin \pi \left(x + y \right), -\sin \pi \left(x + y \right) \right), \\
p &= \frac{1}{\pi^2} \sin \pi \left(x + y \right).
\end{aligned}
$$

Test Function #2 (F2)

$$
\begin{aligned}
\mathbf{u} &= \left(\left(x^4 - 2x^3 + x^2 \right) \left(4y^3 - 6y^2 + 2y \right), - \left(4x^3 - 6x^2 + 2x \right) \left(y^4 - 2y^3 + y^2 \right) \right), \\
p &= x^5 + y^5,
\end{aligned}
$$

adjusting $\mathbf{f}$ so that $[\mathbf{u}, p]$ is a solution to (1) and (3). Note that in both cases the incompressibility condition (2) is satisfied. Also, $\mathbf{u}|_{\partial\Omega} = 0$ for F2 but not for F1.

In all the experiments, we imposed uniform grids on Ω consisting of isosceles right triangles as shown in Figure 1. These ranged from a 13×13 "coarse" grid to a 25×25 grid. In Table 1,
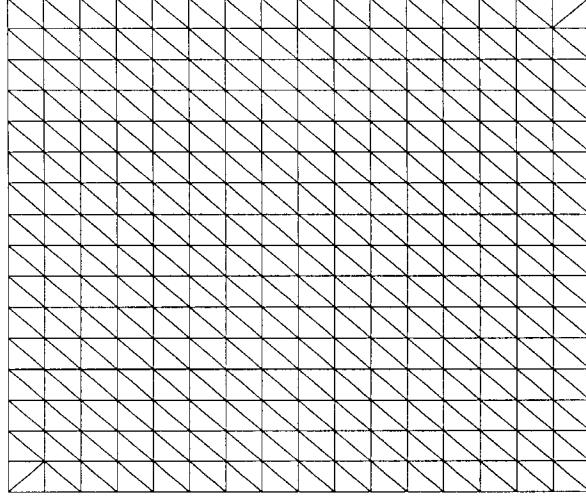
Figure 1. 17×17 grid.

Table 1. Dimensions.

Grid	13×13	17×17	21×21
N_T	288	512	800
dim $\mathbf{V}_k^2$	1440	2560	4000
dim $\mathbf{V}_k^3$	2592	4608	7200
dim $\mathbf{P}_h^2$	169	289	441

Table 2. (F1), $r_1 = r_2 = 2$, Re $= 1000$, $\gamma = 50$.

h^{-1}	$\|E(u)\|_{L^2}$		$\|E(u)\|_{1,k}$		$\|E(p)\|_{0,h}$	
	Error	Rate	Error	Rate	Error	Rate
6	$0.271420E - 02$		$0.218233E + 00$		$0.118079E - 01$	
8	$0.109088E - 02$	3.168	$0.154478E + 00$	1.201	$0.648388E - 02$	2.084
10	$0.581889E - 03$	2.816	$0.121085E + 00$	1.091	$0.411995E - 02$	2.032
12	$0.361743E - 03$	2.607	$0.999393E - 01$	1.053	$0.285344E - 02$	2.015
14	$0.247176E - 03$	2.471	$0.852042E - 01$	1.035	$0.209331E - 02$	2.010
16	$0.179910E - 03$	2.379	$0.743038E - 01$	1.025	$0.160110E - 02$	2.007
18	$0.137106E - 03$	2.307	$0.659013E - 01$	1.019	$0.126423E - 02$	2.006
20	$0.108069E - 03$	2.259	$0.592172E - 01$	1.015	$0.102357E - 02$	2.004
22	$0.875685E - 04$	2.207	$0.537693E - 01$	1.013	$0.845668E - 03$	2.003
24	$0.724353E - 04$	2.180	$0.492433E - 01$	1.011	$0.710444E - 03$	2.002

we show the subsequent number of triangles(N_T) and the dimensions of the finite-element spaces corresponding to the linear-linear and quadratic-linear combinations for the velocity and the pressure.

In Tables 2 and 3, we exhibit the errors $\|\mathbf{u} - \mathbf{u}_k\|_{L^2}$, $\|\mathbf{u} - \mathbf{u}_k\|_{1,k}$, $\|p - p_h\|_{0,h}$, respectively, and the corresponding convergence rates for the first test function (F1). The convergence rate in these tables and in those that follow is computed according to the formula,

$$\text{Rate} = \ln\left(\frac{E_1}{E_2}\right) \bigg/ \ln\left(\frac{h_1}{h_2}\right),$$

where E_i is the discretization error corresponding to mesh size h_i. These tables differ slightly

Table 3. (F1), $r_1 = 3$, $r_2 = 2$, Re $= 1000$, $\gamma = 50$.

h^{-1}	$\|E(u)\|_{L^2}$		$\|E(u)\|_{1,k}$		$\|E(p)\|_{0,h}$	
	Error	Rate	Error	Rate	Error	Rate
6	0.317855E − 02		0.245591E + 00		0.118134E − 01	
8	0.116768E − 02	3.481	0.130543E + 00	2.197	0.648448E − 02	2.085
10	0.565684E − 03	3.248	0.818998E − 01	2.089	0.411983E − 02	2.033
12	0.319130E − 03	3.140	0.564581E − 01	2.040	0.285317E − 02	2.015
14	0.198322E − 03	3.086	0.413794E − 01	2.016	0.209301E − 02	2.010
16	0.131876E − 03	3.056	0.316914E − 01	1.998	0.160085E − 02	2.008
18	0.922359E − 04	3.035	0.250966E − 01	1.981	0.126404E − 02	2.006
20	0.670863E − 04	3.022	0.203939E − 01	1.969	0.102344E − 02	2.004
22	0.503381E − 04	3.013	0.169171E − 01	1.961	0.845569E − 03	2.003
24	0.388012E − 04	2.992	0.142719E − 01	1.954	0.710366E − 03	2.002

Table 4. (F2), $r_1 = 2$, $r_2 = 2$, Re $= 1000$, $\gamma = 50$.

h^{-1}	$\|E(u)\|_{L^2}$		$\|E(u)\|_{1,k}$		$\|E(p)\|_{0,h}$	
	Error	Rate	Error	Rate	Error	Rate
6	0.297854E − 01		0.115226E + 01		0.117173E + 00	
8	0.123317E − 01	3.065	0.630035E + 00	2.099	0.669895E − 01	1.944
10	0.626874E − 02	3.032	0.395389E + 00	2.088	0.432210E − 01	1.964
12	0.364048E − 02	2.981	0.270867E + 00	2.075	0.301522E − 01	1.975
14	0.232107E − 02	2.920	0.197128E + 00	2.061	0.222154E − 01	1.982
16	0.158553E − 02	2.854	0.149943E + 00	2.049	0.170404E − 01	1.986
18	0.114169E − 02	2.788	0.117955E + 00	2.037	0.134813E − 01	1.989
20	0.856911E − 03	2.723	0.952851E − 01	2.026	0.109299E − 01	1.991
22	0.664818E − 03	2.663	0.786389E − 01	2.015	0.903916E − 02	1.993
24	0.529843E − 03	2.608	0.660586E − 01	2.003	0.759932E − 02	1.994

Table 5. (F2), $r_1 = 3$, $r_2 = 2$, Re $= 1000$, $\gamma = 50$.

h^{-1}	$\|E(u)\|_{L^2}$		$\|E(u)\|_{1,k}$		$\|E(p)\|_{0,h}$	
	Error	Rate	Error	Rate	Error	Rate
6	0.469292E − 01		0.303473E + 01		0.115756E + 00	
8	0.192761E − 01	3.093	0.167690E + 01	2.062	0.663451E − 01	1.935
10	0.968136E − 02	3.086	0.106024E + 01	2.054	0.428593E − 01	1.958
12	0.552236E − 02	3.079	0.729609E + 00	2.050	0.299221E − 01	1.971
14	0.343954E − 02	3.071	0.532077E + 00	2.048	0.220567E − 01	1.978
16	0.228433E − 02	3.065	0.404194E + 00	2.059	0.169248E − 01	1.983
18	0.159355E − 02	3.057	0.317075E + 00	2.061	0.133927E − 01	1.987
20	0.115516E − 02	3.054	0.255067E + 00	2.065	0.108600E − 01	1.990
22	0.863943E − 03	3.048	0.208263E + 00	2.127	0.898302E − 02	1.991
24	0.663177E − 03	3.039	0.174722E + 00	2.018	0.755298E − 02	1.993

from the corresponding tables in [8] due to a different scaling of the velocity basis functions. Tables 4 and 5 are for the second test function (F2). Tables 2 and 4 correspond to $r_1 = r_2 = 2$ and Tables 3 and 5 to $r_1 = 3$, $r_2 = 2$. The prevailing values of the Reynolds number Re $= 1/\nu$ and γ are as shown. The rates are seen to conform to theoretical predictions. Note that the rate for the L^2-error for the velocity in Tables 2 and 4 is slightly larger than the predicted value of 2. Also, the errors for the pressure are the same for both values of r_1.

(a). (F2) Re = 100.   (b). Re = 1000.
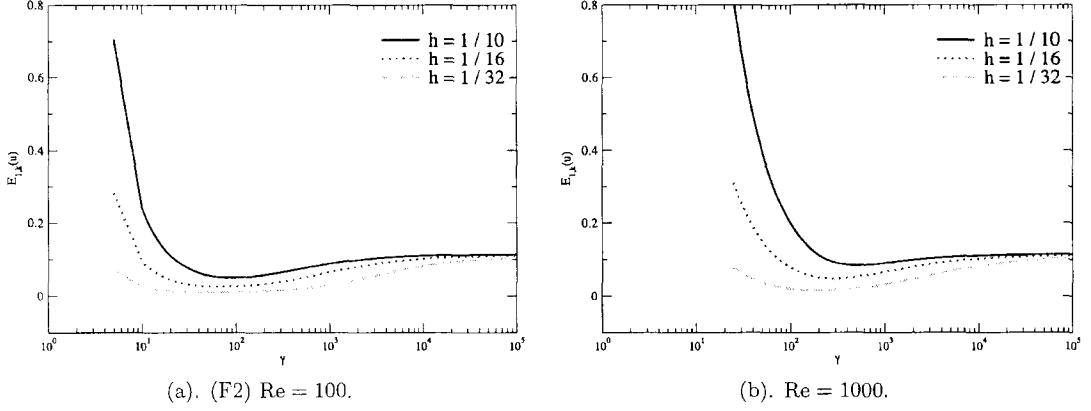
Figure 2. $E_{1,k}(u)$ error.

(a)   (b)

(c)   (d)
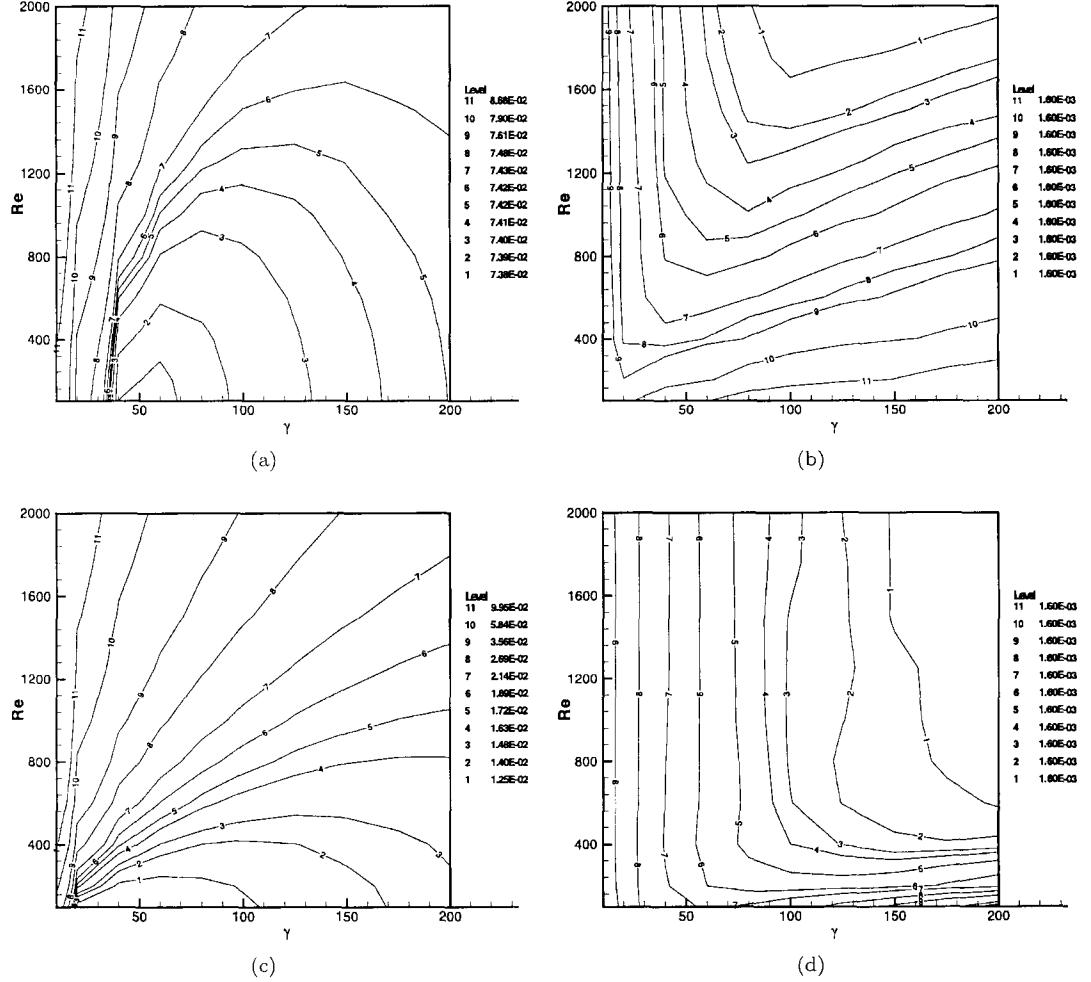
Figure 3. Level curves for the errors: $E_{1,k}(u)$ (a,c), $E_{0,h}(p)$ (b,d).

Next, we study the effect of the parameter γ on the errors. Figures 2a and 2b display, in logarithmic scale in the γ-axis, the behavior of the $E_{1,k}(u)$-error with respect to γ for three values of h, $h = 1/10$, $1/16$, $1/32$, $r_1 = r_2 = 2$ and two different values of Re. We notice that in all cases there is a critical value of γ which minimizes the error. It is also worth noting that the errors become unbounded as $\gamma \rightarrow 0^+$, given that the bilinear form a_k^γ becomes singular for

small γ. On the other hand, the errors increase monotonically to an asymptotic limit as $\gamma \to \infty$. Further, the pressure error does not seem to be affected by the choice of γ, Figures 3b and 3d.

A very interesting issue is the dependence of the errors on Re and γ. In Figure 3, we show the level curves for the errors in terms of these two parameters. In these experiments, we took $h = 1/16$. Figures 3a and 3b correspond to $r_1 = r_2 = 2$ while Figures 3c and 3d correspond to $r_1 = 3$, $r_2 = 2$. First, we observe that while the error for the velocity increases with Re, the opposite happens with the pressure. However, the variation in the latter is rather insignificant. On the other hand, for a fixed value of Re, the shapes of the level curves for the velocity indicate the existence of an optimal value of γ in the sense of minimizing the error. This is consistent with the data reported in Figure 2. Further from Figures 3a and 3c we can conclude that we may choose "optimal" values for γ using the formulas $\gamma \sim 43 + \text{Re}/15$ for $r_1 = r_2 = 2$ and $\gamma \sim \text{Re}/4$ for $r_1 = 3$, $r_2 = 2$.

3.3. The Navier-Stokes Problem

The same type of experiments, as in the Stokes problem, were performed also in this case. The starting values for the Newton iteration were the solution of the corresponding Stokes problem. This strategy is followed in all the experiments reported here. The scheme converged in two or three iterations with tolerance TOL $= 10^{-5}$.

In Table 6, the errors and the convergence rates are displayed. The rates are in good agreement with the predicted theoretical rates.

Table 6. (F2), $r_1 = 3$, $r_2 = 2$, Re $= 100$, $\gamma = 40$.

h^{-1}	$\|E(u)\|_{L^2}$		$\|E(u)\|_{1,k}$		$\|E(p)\|_{0,h}$	
	Error	Rate	Error	Rate	Error	Rate
6	$0.578271E - 02$		$0.370618E + 00$		$0.116888E + 00$	
8	$0.237820E - 02$	3.089	$0.205087E + 00$	2.057	$0.668611E - 01$	1.942
10	$0.119497E - 02$	3.084	$0.129761E + 00$	2.051	$0.431534E - 01$	1.962
12	$0.682084E - 03$	3.075	$0.893687E - 01$	2.045	$0.301121E - 01$	1.974
14	$0.425040E - 03$	3.068	$0.652329E - 01$	2.042	$0.221895E - 01$	1.981
16	$0.282543E - 03$	3.058	$0.496940E - 01$	2.038	$0.170225E - 01$	1.985
18	$0.197238E - 03$	3.052	$0.391058E - 01$	2.034	$0.134687E - 01$	1.988
20	$0.143170E - 03$	3.041	$0.315710E - 01$	2.031	$0.109204E - 01$	1.991
22	$0.107350E - 03$	3.021	$0.260173E - 01$	2.030	$0.903191E - 02$	1.992
24	$0.827219E - 04$	2.995	$0.218098E - 01$	2.027	$0.759365E - 02$	1.993

We investigate further the choice of the trilinear form (13). Indeed, there are two alternatives trilinear forms. Namely, we can set

$$b_A(\mathbf{u}, \mathbf{v}, \mathbf{w}) = b_1(\mathbf{u}, \mathbf{v}, \mathbf{w}), \tag{19}$$

where $b_1(\cdot, \cdot, \cdot)$ is defined by (13) or even simpler, we can take

$$b_B(\mathbf{u}, \mathbf{v}, \mathbf{w}) = \sum_{i=1}^{d_k} \int_{\Omega_i} u_\ell^{(i)} \frac{\partial v_m^{(i)}}{\partial x_\ell} w_m^{(i)} \, dx. \tag{20}$$

These trilinear forms require less computational work than b. However, we do not have yet convergence results for these forms. Tables 7 and 8 correspond to Table 6 for these trilinear forms. The errors and the convergence from these tables show that there is no essential difference between these forms.

Table 7. (F2), (b_B), $r_1 = 3$, $r_2 = 2$, Re $= 100$, $\gamma = 40$.

h^{-1}	$\|E(u)\|_{L^2}$		$\|E(u)\|_{1,k}$		$\|E(p)\|_{0,h}$	
	Error	Rate	Error	Rate	Error	Rate
6	0.576702E − 02		0.368896E + 00		0.116890E + 00	
8	0.237681E − 02	3.081	0.204787E + 00	2.046	0.668611E − 01	1.942
10	0.119479E − 02	3.082	0.129681E + 00	2.048	0.431532E − 01	1.962
12	0.682171E − 03	3.074	0.893361E − 01	2.044	0.301118E − 01	1.974
14	0.425113E − 03	3.068	0.652241E − 01	2.041	0.221894E − 01	1.981
16	0.282546E − 03	3.059	0.496890E − 01	2.037	0.170227E − 01	1.985
18	0.197164E − 03	3.055	0.391031E − 01	2.034	0.134690E − 01	1.988
20	0.143185E − 03	3.036	0.315679E − 01	2.032	0.109206E − 01	1.991
22	0.107339E − 03	3.023	0.260125E − 01	2.031	0.903200E − 02	1.992
24	0.827290E − 04	2.993	0.218075E − 01	2.026	0.759362E − 02	1.994

Table 8. (F2), (b_A), $r_1 = 3$, $r_2 = 2$, Re $= 100$, $\gamma = 40$.

h^{-1}	$\|E(u)\|_{L^2}$		$\|E(u)\|_{1,k}$		$\|E(p)\|_{0,h}$	
	Error	Rate	Error	Rate	Error	Rate
6	0.576769E − 02		0.370237E + 00		0.116876E + 00	
8	0.237663E − 02	3.082	0.205006E + 00	2.055	0.668597E − 01	1.941
10	0.119412E − 02	3.084	0.129729E + 00	2.051	0.431533E − 01	1.962
12	0.681936E − 03	3.073	0.893497E − 01	2.045	0.301120E − 01	1.974
14	0.424991E − 03	3.068	0.652268E − 01	2.041	0.221895E − 01	1.981
16	0.282497E − 03	3.058	0.496858E − 01	2.038	0.170226E − 01	1.985
18	0.197122E − 03	3.055	0.391052E − 01	2.033	0.134690E − 01	1.988
20	0.143145E − 03	3.037	0.315697E − 01	2.032	0.109207E − 01	1.991
22	0.107320E − 03	3.022	0.260128E − 01	2.031	0.903201E − 02	1.992
24	0.827147E − 04	2.993	0.218085E − 01	2.026	0.759362E − 02	1.994

3.4. Benchmark Problems

In literature, two problems have become standard benchmarks for testing numerical schemes solving the equations of fluid flow. These are: the flow in a *driven cavity*, [17,18] and the flow in a *backward facing step* [18,19]. In both cases, we solve the corresponding stationary problem.

3.4.1. Driven cavity

In this test problem the fluid is driven horizontally on the upper side of a square cavity with side α. The Reynolds number here is defined to be Re $= \alpha U / \nu$, where U is the horizontal velocity on the upper side and ν is the viscosity of the fluid. For simplicity, we take $\alpha = 1$ and $U = 1$ on the top side of the cavity. The velocity on the other sides of the cavity is taken to be zero. The main characteristic of the flow, shown in Figure 4a, is the creation of a principal vortex (PV) close to geometric center of the cavity and secondary vortices, (LV), (RV$_1$), (RV$_2$), and (TV), on the bottom left and right corners and on the upper right corner, respectively.

To study the flow, we put a nonuniform grid, shown in Figure 4b, concentrated at the corners and walls of the cavity. The mesh consists of 2194 triangles resulting in 10970 velocity unknowns and 1178 pressure unknowns, where linear elements were used for the velocity and the pressure. We tested our code for the following values of Re-number,

$$\text{Re} = 100, 400, 1000, 2000, 3200, 5000, 7500, 10000.$$
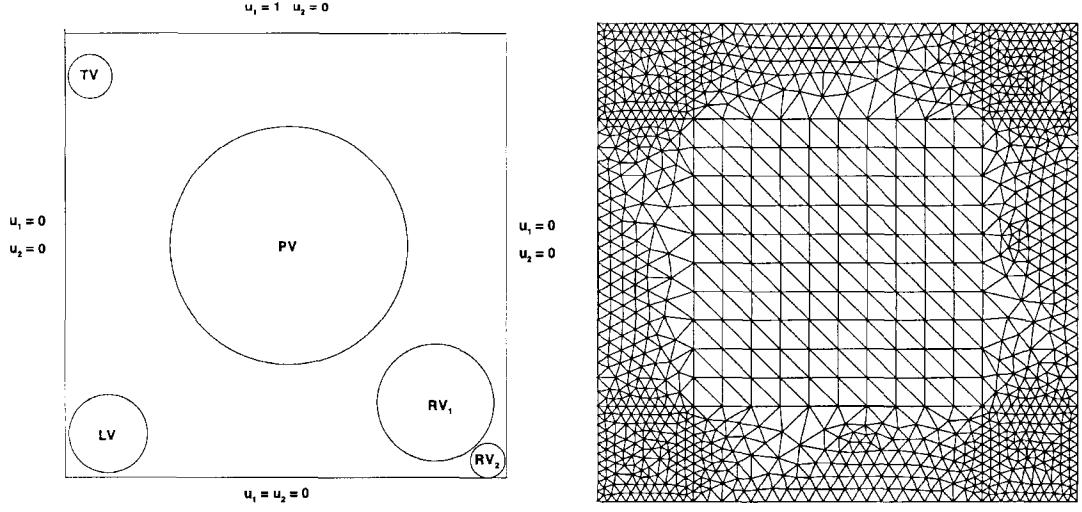
(a). Structure of the flow.

(b). The mesh.

Figure 4. The geometry and the mesh.

Table 9. Values of γ and ℓ_n.

Re	γ	ℓ_n
100	50	2
400	60	2
1000	80	3
2000	130	3
3200	160	3
5000	200	3
7500	270	3
10000	340	3

Table 10. Centers of the vortices.

Re	PV	RV_1	LV	TV	RV_2
100	0.61778 0.75016	0.94354 0.05279	0.02554 0.02777	—	—
400	0.55889 0.60251	0.87982 0.11363	0.02872 0.04134	—	—
1000	0.53356 0.56658	0.85934 0.09987	0.07371 0.06751	—	—
2000	0.52371 0.54695	0.85427 0.09608	0.07699 0.10153	—	—
3200	0.51706 0.54042	0.83082 0.08514	0.07497 0.11394	0.04785 0.89401	—
5000	0.51174 0.53799	0.81163 0.08171	0.07156 0.11661	0.05825 0.90593	—
7500	0.50803 0.53669	0.79269 0.07807	0.06835 0.12368	0.06225 0.91054	0.94042 0.03996
10000	0.50697 0.53565	0.74692 0.05805	0.06274 0.15549	0.06371 0.91069	0.93981 0.07856

To compute the solution for the final value of Re-number we proceed as follows. We compute the solution for Re = 100 using as initial value for Newton's iteration the solution of the corresponding Stokes problem. The necessary Newton iterations (ℓ_N) were taken to be 5 and our convergence criterion was that the difference, measured in the L^2 norm, of two successive iterates be less than 10^{-5}. Now, to compute the solution for the next value of Reynolds number, we use as starting value for Newton's iteration the solution of the previous value of Re-number. In Table 9, we show the values of γ and ℓ_n needed to obtain the solution for the given Re-number following the above process.

Typically for this benchmark problem part of the standard output includes the following.

- The streamlines in the whole domain.
- The location of the centers of the vortices.
- The profiles of u_1 along $x = 1/2$ and u_2 along $y = 1/2$.

In Table 10, we list the locations of the centers of the vortices. The streamlines in the whole domain as well as in the corners are shown in Figures 5 and 6 for the various values of Re-number. In Figure 7, we give the profiles of u_1 along $x = 1/2$ and u_2 along $y = 1/2$. In Table 11, we

(a). Re = 100.

(b). Re = 400.

(c). Re = 1000.

(d). Re = 2000.
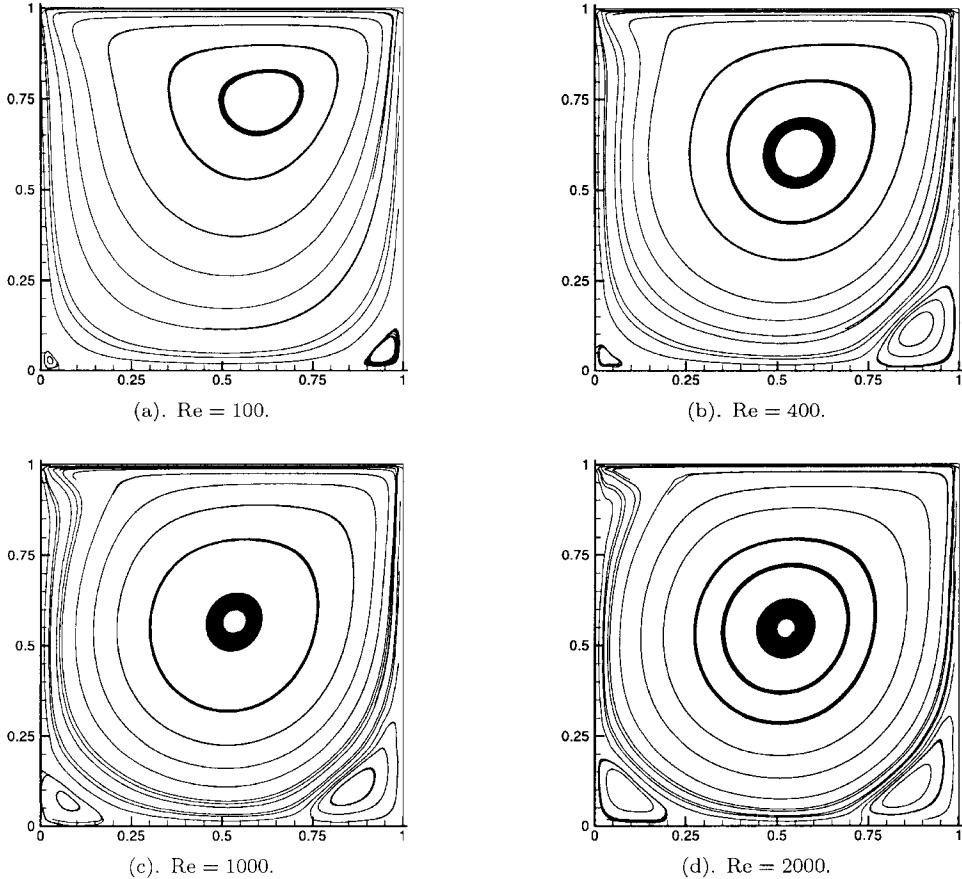
Figure 5. Streamlines.

(a). Re = 3200.

(b). Re = 5000.

Figure 6. Streamlines.

(c). Re = 7500.   (d). Re = 10000.

Figure 6. (cont.)

(a). u_1 along $x = 1/2$.   (b). u_2 along $y = 1/2$.
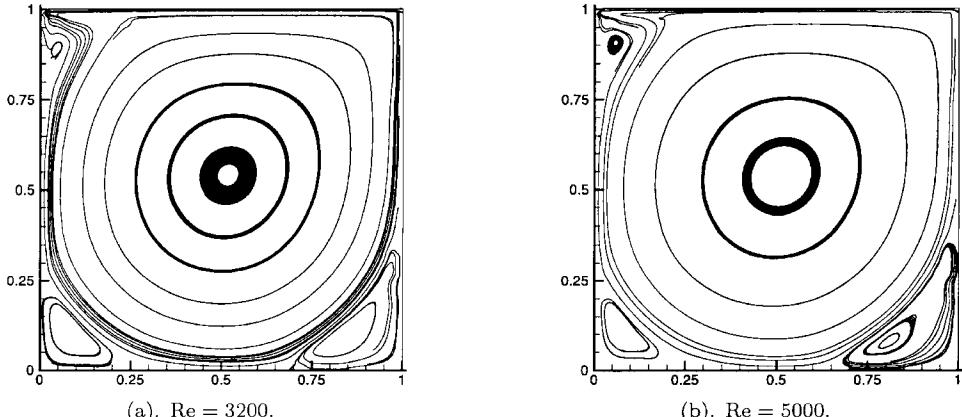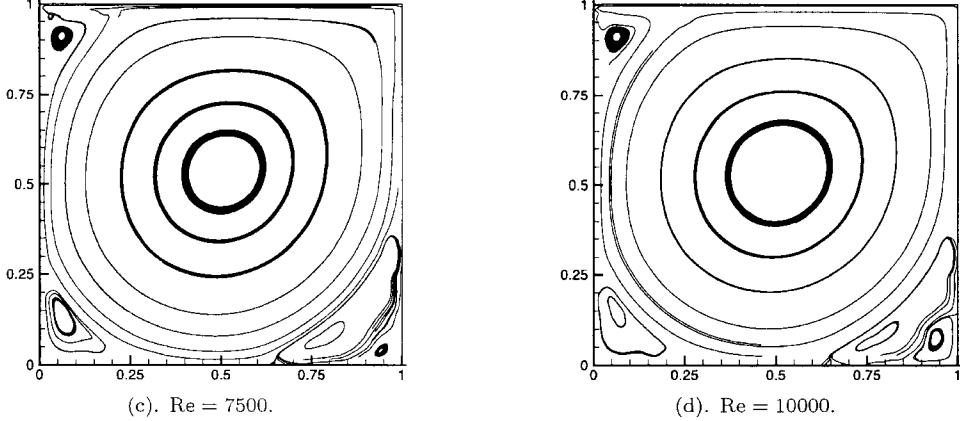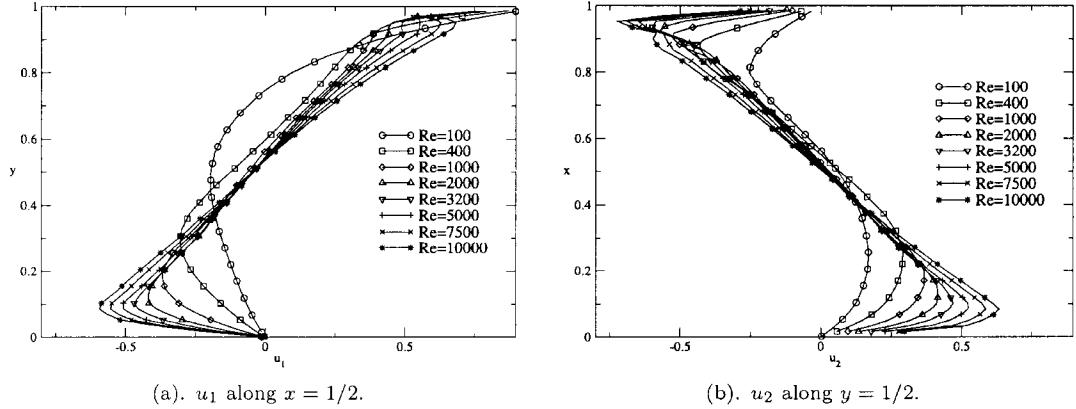
Figure 7. Velocity profiles.

Table 11. Location of vortex centers : (a) this work, (b) [20], (c) [21], (d) [22], (e) [23], (f) [24], (g) [25].

Re		PV	RV$_1$	LV
	a	0.61778 0.75016	0.94354 0.05279	0.02554 0.02777
	b	0.6172 0.7344	0.9453 0.0625	0.0313 0.0391
	c	0.6188 0.7375	0.9375 0.0563	0.0375 0.0313
100	d	0.6167 0.7417	0.9417 0.0500	0.0333 0.0250
	e	0.6196 0.7373	0.9451 0.0627	0.0392 0.0353
	f	0.6172 0.7383	0.9414 0.0625	0.0352 0.0352
	g	0.6152 0.7383	0.9493 0.0587	0.0275 0.0352
	a	0.55889 0.60251	0.87982 0.11363	0.02872 0.04134
	b	0.5547 0.6055	0.8906 0.1250	0.0508 0.0469
	c	0.5563 0.6000	0.8875 0.1188	0.0500 0.0500
400	d	0.5571 0.6071	0.8857 0.1143	0.0500 0.0429
	e	0.5608 0.6078	0.8902 0.1255	0.0549 0.0510
	f	0.5547 0.6055	0.8867 0.1250	0.0508 0.0469
	g	0.5588 0.6053	0.8906 0.1172	0.0537 0.0425

compare the locations of the centers of the main vortices (PV), (RV$_1$), (LV) with the results reported in [20–25]. We have an overall agreement of our solutions with respect to the shape and location of the three main vortices for all values of Re-number up to Re = 3200. For Re ≥ 5000, there are small differences between our solutions, which are mainly on the location and shape of

Table 11. (cont.)

Re		PV	RV$_1$	LV
1000	a	0.53356 0.56658	0.85934 0.09987	0.07371 0.06751
	b	0.5313 0.5625	0.8594 0.1094	0.0859 0.0781
	c	0.5438 0.5625	0.8625 0.1063	0.0750 0.0813
	d	0.5286 0.5643	0.8643 0.1071	0.0857 0.0714
	e	0.5333 0.5647	0.8667 0.1137	0.0902 0.0784
	f	0.5313 0.5664	0.8633 0.1133	0.0820 0.0781
	g	0.5352 0.5664	0.8691 0.1128	0.0859 0.0741
2000	a	0.52371 0.54695	0.85427 0.09608	0.07699 0.10153
	c	0.5250 0.5500	0.8375 0.0938	0.0875 0.1063
	e	0.5255 0.5490	0.8471 0.0980	0.0902 0.1059
	f	0.5195 0.5469	0.8438 0.0977	0.0859 0.1016
	g	0.5234 0.5484	0.8477 0.0977	0.0850 0.1010
3200	a	0.51706 0.54042	0.83082 0.08514	0.07497 0.11394
	b	0.5165 0.5469	0.8125 0.0859	0.0859 0.1094
	f	0.5156 0.5391	0.8242 0.0859	0.0820 0.1172
	g	0.5195 0.5430	0.8320 0.0898	0.0828 0.1152
5000	a	0.51174 0.53799	0.81163 0.08171	0.07156 0.11661
	b	0.5117 0.5352	0.8086 0.0742	0.0703 0.1376
	c	0.5125 0.5313	0.8500 0.0813	0.0625 0.1563
	e	0.5176 0.5373	0.8078 0.0745	0.0784 0.1373
	f	0.5156 0.5352	0.8008 0.0742	0.0742 0.1328
	g	0.5156 0.5352	0.8086 0.0742	0.0723 0.1391
7500	a	0.50803 0.53669	0.79269 0.07807	0.06835 0.12368
	b	0.5117 0.5322	0.7813 0.0625	0.0645 0.1504
	e	0.5176 0.5333	0.7922 0.0667	0.0706 0.1529
	f	0.5117 0.5313	0.7813 0.0664	0.0625 0.1523
10000	a	0.50697 0.53565	0.74692 0.05805	0.06274 0.15549
	b	0.5117 0.5333	0.7656 0.0586	0.0586 0.1641
	d	0.5140 0.5307	0.7877 0.0615	
	f	0.5117 0.5313	0.7578 0.0586	0.0586 0.1602

the secondary vortices. Overall we can say that the present method provides adequate results even for fairly large Re-number using much coarser grids (34×34) compared to that of (129×129) up to (257×257) used by the aforementioned works.

3.4.2. Backward Facing Step

We turn our attention to the second benchmark problem: the flow in a backward facing step [18,19]. The geometry of the problem is shown in Figure 8. At the entrance a parabolic profile is prescribed, while the velocity is taken to be zero on the sides. At the exit, a parabolic profile is also given so that the total flux along the boundary is zero. Here, we assume that the flow is fully developed at the exit.
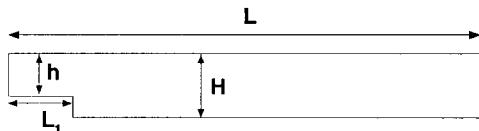

Figure 8. The geometry.

Alternatively, a "Neumann" type boundary condition of the form, $\nu\frac{\partial \mathbf{u}}{\partial \mathbf{n}} = p\mathbf{n}$ can be also imposed at the exit. Indeed the formulation allows us to incorporate this type of boundary condition quite easily. Let $\partial\Omega_N$ and $\partial\Omega_D$ denote the part of the boundary where the Neumann and Dirichlet conditions are applied respectively. Then, we modify the bilinear form $a_k^\gamma(\cdot,\cdot)$ to

$$a_{k,D}^\gamma(\mathbf{u},\mathbf{v}) = \sum_{i=1}^{d_k}\left\{ (\nabla\mathbf{u}^{(i)},\nabla\mathbf{v}^{(i)})_{\Omega_i} + \sum_{j\in\mathcal{N}_i}\tau_{ij}\left[-\left\langle\frac{\partial\mathbf{u}^{(i)}}{\partial n},\mathbf{v}^{(i)}-\mathbf{v}^{(j)}\right\rangle_{\partial\Omega_{i,j}}\right.\right.$$

$$-\left\langle\frac{\partial\mathbf{v}^{(i)}}{\partial n},\mathbf{u}^{(i)}-\mathbf{u}^{(j)}\right\rangle_{\partial\Omega_{i,j}} + \gamma k_i^{-1}\left\langle\mathbf{u}^{(i)}-\mathbf{u}^{(j)},\mathbf{v}^{(i)}-\mathbf{v}^{(j)}\right\rangle_{\partial\Omega_{i,j}}\Big] - \left\langle\frac{\partial\mathbf{u}^{(i)}}{\partial n},\mathbf{v}^{(i)}\right\rangle_{\partial\Omega_i^{e,D}}$$

$$\left.-\left\langle\frac{\partial\mathbf{v}^{(i)}}{\partial n},\mathbf{u}^{(i)}\right\rangle_{\partial\Omega_i^{e,D}} + \gamma k_i^{-1}\left\langle\mathbf{u}^{(i)},\mathbf{v}^{(i)}\right\rangle_{\partial\Omega_i^{e,D}}\right\} - \sum_{i=1}^{d_k}\left\langle\frac{\partial\mathbf{u}^{(i)}}{\partial n},\mathbf{v}^{(i)}\right\rangle_{\partial\Omega_i^{e,N}}$$

where $\partial\Omega_i^{e,D} = \Omega_i\cap\partial\Omega_D$ and $\partial\Omega_i^{e,N} = \Omega_i\cap\partial\Omega_N$. We replace the last term in $a_{k,D}^\gamma(\cdot,\cdot)$ by $(1/\nu)\langle\mathbf{u}\cdot\mathbf{n},p\rangle$. Also, notice that if $\mathbf{u}$ is smooth over Ω and solenoidal then,

$$(\mathbf{u},\nabla q) = \langle\mathbf{g}\cdot\mathbf{n},q\rangle_{\partial\Omega_D} + \langle\mathbf{u}\cdot\mathbf{n},q\rangle_{\partial\Omega_N}$$

Hence, in this case, we define the Galerkin approximation of the stationary Navier-Stokes problem (1)–(3) as the unique solution $[\mathbf{u}_k,p_h]\in\mathbf{V}_k^{r_1}\times P_h^{r_2}/R$ of

$$\nu a_{k,D}^\gamma(\mathbf{u}_k,\mathbf{v}) + (\mathbf{u}_k,\nabla q) + (\mathbf{v},\nabla p_h) - \langle\mathbf{u}_k\cdot\mathbf{n},q\rangle_{\partial\Omega_N} - \langle\mathbf{v}\cdot\mathbf{n},p_h\rangle_{\partial\Omega_N}$$

$$+b_B(\mathbf{u}_k,\mathbf{u}_k,\mathbf{v}) = F_{NS}^D[\mathbf{v},q],\quad \forall[\mathbf{v},q]\in\mathbf{V}_k^{r_1}\times P_h^{r_2}/R,$$

where

$$F_{NS}^D([\mathbf{v},q]) = (\mathbf{f},\mathbf{v}) - \nu\sum_{i=1}^{d_k}\left\langle\frac{\partial\mathbf{v}^{(i)}}{\partial n}-\gamma k_i^{-1}\mathbf{v}^{(i)},\mathbf{g}\right\rangle_{\partial\Omega_i^{e,D}} + \langle\mathbf{g}\cdot\mathbf{n},q\rangle_{\partial\Omega_D}.$$

In the case of the Stokes problem the modified variational formulation preserves its symmetry.

The Reynolds–number in this case is defined as $\mathrm{Re} = (U_{\max}(H-h))/\nu$ where $U_{\max}$ is the maximum velocity at the entrance, $H-h$ determines the height of the step and ν is the viscosity of the fluid. The main characteristic of the flow is the creation of a vortex right after the step.

To study the flow, we put a nonuniform grid on the domain, concentrated mainly at the entrance and on the recirculation region. The mesh consists of 1784 triangles resulting in 8920 velocity unknowns and 956 pressure unknowns. We use linear elements for the velocity and for the pressure approximations. To test our code, we have chosen the following set of parameters [19],

$$L = 22,\qquad L_1 = 3,\qquad H = 1.5,\qquad h = 1,$$

along with the following boundary conditions,

$$\mathbf{u} = -\frac{4}{h^2}(y-H+h)(y-H),\qquad \text{at the entrance } (U_{\max}=1),$$

$$\mathbf{u} = -\frac{4}{H^3}y(y-H),\qquad \text{at the exit,}$$

$$\mathbf{u} = 0,\qquad \text{on the sides.}$$

The values of Re-number tested were: $\mathrm{Re} = 50, 150$. The initial value for Newton's iteration was the solution of the associated Stokes problem. The values of γ and ℓ_N needed to obtain the solution for the given Re-number are given in Table 12.

Table 12. Values of γ and ℓ_n.

Re	γ	ℓ_n
50	55	2
150	100	3

Table 13. Length of recirculation region.

| Re	Length
50	2.95
150	6.08
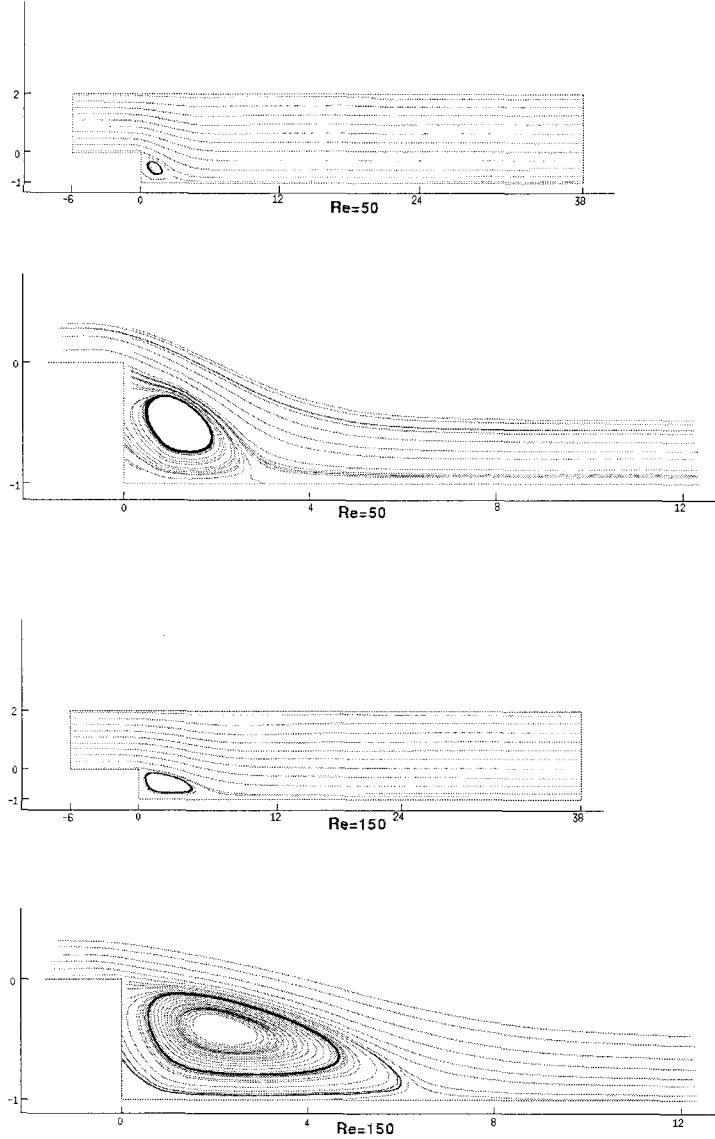
Figure 9. Streamliners, Re = 50, 150.

The output for this flow consists in part of the following nondimensionalized values.

- Streamline plots on the whole domain and in the recirculation region.
- Pressure level plots on the whole domain and in the recirculation region with $\bar{p} = \text{Re} U_{\max}^2 p$ and $p = 0$ at the step corner.
- Length of the recirculation region.

The length of the recirculation region is given in Table 13. In Figure 9, the streamlines in the whole and in the recirculation area are plotted for Re = 50, 150, respectively. The corresponding pressure contour plots are shown in Figure 10. In all plots, the axes have been nondimensionalized by $1/(H - h)$ and the origin is at the step corner. We compared our solution with the solution of the actual experiment reported in [19]. For both values of Re-number our solutions agree very well with respect to the vortex shape and the length of the recirculation region. In particular,
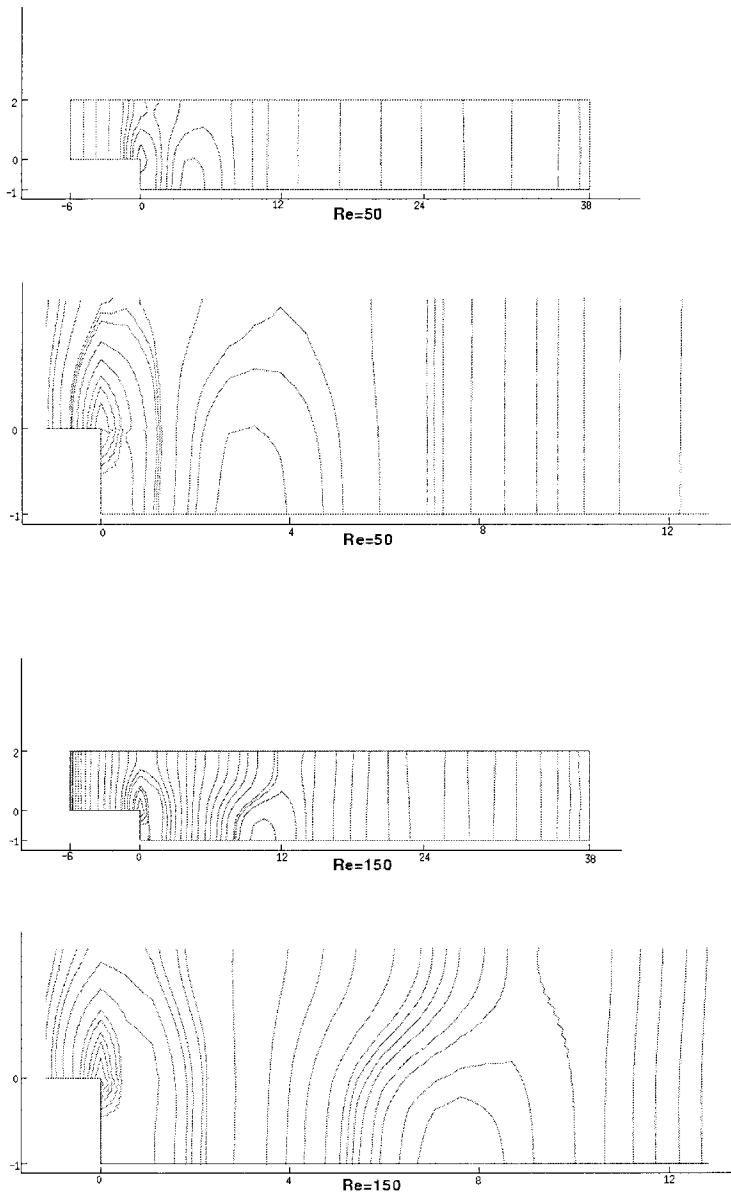
Figure 10. Pressure contours, Re = 50, 150.

the computed length of the recirculation region, for Re = 50 and Re = 150 differs only by 0.05 and 0.08, respectively.

The above results were obtained with the parabolic exit profile. We also implemented the boundary condition $\nu\frac{\partial \mathbf{u}}{\partial \mathbf{n}} = p\mathbf{n}$. However, the numerical results agreed very closely to those obtained with the parabolic profile.

4. CONCLUSION

The numerical results presented herein confirm the analytical results of [1] and [2]. They also highlight two important characteristics of the method.

(1) The results of the two benchmark problems show that the method can accurately simulate fluid flow problems and do so efficiently as evidenced by the relatively small number of elements. We believe that the efficiency can be further enhanced by the inclusion of adaptive mesh selection. The adoption of Multigrid for solving the systems of equations is another way to reduce run times. Both of these features are being currently developed.

(2) The method is sufficiently flexible to handle a variety of B.C.'s including Dirichlet, Neumann as well as other esoteric B.C.s such as $\nu \frac{\partial \mathbf{u}}{\partial \mathbf{n}} = p\mathbf{n}$.

REFERENCES

1. G. Baker, W. Jureidini and O. Karakashian, Piecewise solenoidal vector fields and the Stokes problem, *SIAM Journal of Numerical Analysis* **27**, 1466–1485, (1990).
2. O. Karakashian and W. Jureidini, A nonconforming finite element method for the stationary Navier-Stokes equations, *SIAM Journal of Numerical Analysis* **35**, 93–120, (1998).
3. D.N. Arnold, An interior penalty finite element method with discontinuous elements, *SIAM Journal Numerical Analysis* **19**, 742–760, (1982).
4. M.F. Wheeler, An elliptic collocation-finite element method with interior penalties, *SIAM Journal Numerical Analysis* **15**, 152–161, (1978).
5. J. Douglas Jr. and T. Dupont, Interior penalty procedures for elliptic and parabolic Galerkin methods, In *Lecture Notes in Physics, Volume 58*, Springer-Verlag, (1976).
6. J.T. Oden and C.E. Baumann, A conservative DGM for convection-diffusion and Navier-Stokes problems, In *Proceedings of the International Symposium on the Discontinuous Galerkin Method, Springer Lecture Notes in Computational Science and Engineering*, (Edited by B. Cockburn *et al.*), pp. 179–196, (1999).
7. T. Katsaounis, On Fully discrete Galerkin approximations for the incompressible Navier-Stokes equations, Ph.D. Thesis, University of Tennessee, Knoxville, TN, (1994).
8. O. Karakashian and T. Katsaounis, A discontinuous Galerkin method for the incompressible Navier-Stokes equations, In *Proceedings of the International Symposium on the Discontinuous Galerkin Method, Springer Lecture Notes in Computational Science and Engineering*, (Edited by B. Cockburn *et al.*), pp. 157–166, (1999).
9. R. Adams, *Sobolev Spaces*, Academic Press, (1975).
10. P. Ciarlet, *The Finite Element Method for Elliptic Problems*, North-Holland, (1980).
11. I. Babuska and M. Zlamal, Nonconforming elements in the finite element method with penalty, *SIAM Journal Numerical Analysis* **10**, 863–875, (1973).
12. G. Baker, Finite element methods for elliptic equations using nonconforming elements, *Mathematics of Computation* **31**, 45–59, (1977).
13. F. Brezzi and J. Douglas, Jr., Stabilized mixed methods for the Stokes problem, *Numerische Mathematik* **53**, 225–235, (1988).
14. T.J.R. Hughes and L.P. Franca, A new finite element formulation for computational fluid dynamics: VII. The Stokes problem with various well-posed boundary conditions: Symmetric formulations that converge for all velocity-pressure spaces., *Computer Methods in Applied Mechanics and Engineering* **65**, 85–96, (1987).
15. Modulef Library, INRIA, France.
16. R. Bramley, An orthogonal projection algorithm for generalized Stokes problem, *Report 1190 CSRD*, (1992).
17. F. Thomasset, *Implementation of Finite Element Methods for Navier-Stokes Equations*, Springer Series in Computational Physics, Springer-Verlag, (1981).
18. O. Pironneau, *Finite Element Methods for Fluids*, Wiley, (1989).
19. K. Morgan, J. Periaux and F. Thomasset, Analysis of laminar flow over a Backward facing step, In *Notes on Numerical Fluid Mechanics, Volume 9*, Fried. Vieweg, Sohn.
20. U. Ghia, K.N. Ghia and C.T. Shin, High-Re solutions for incompressible flow using the Navier-Stokes equations and a multigrid method, *Journal of Computational Physics* **48**, 387–411, (1982).
21. S.P. Vanka, Block-implicit multigrid solution of Navier-Stokes equations in primitive variables, *Journal of Computational Physics* **65**, 138–158, (1986).
22. R. Schreiber and H.B. Keller, Driven cavity flows by efficient numerical techniques, *Journal of Computational Physics* **49**, 310–333, (1983).
23. S. Hou, Q. Zou, S. Chen, G. Doolen and A. Cogley, Simulation of cavity flow by the lattice Boltzmann method, *Journal of Computational Physics* **118**, 329–347, (1995).
24. L.B. Zhang, A second order upwinding finite difference scheme for the steady Navier-Stokes equations in primitive variables in a driven cavity with a multigrid solver, *Mathematical Modeling and Numerical Analysis* **24** (1), 113–150, (1990).
25. C.M. Teixeira, Digital physics simulation of lid-driven cavity flow, *International Journal of Modern Physics C* **8** (4), 685–696, (1997).